RAP Conference Proceedings, vol. 4, pp. 72–77, 2019
ISSN 2466-4626 (online) | doi: 10.37392/RapProc.2019.15
WWW.RAP-PROCEEDINGS.ORG

COMPARISON OF COMPUTATIONAL AND EXPERIMENTAL DOSE RATES IN A NEUTRON ACTIVATION ANALYSIS FACILITY

Jose Rafael Parga[1, 2*], Sheldon Landsberger[2]

[1]Los Alamos National Laboratory, Los Alamos, New Mexico, United States of America
[2]The University of Texas at Austin, Austin, Texas, United States of America

Abstract. *The vast majority of radiation protection guidelines in nuclear facilities usually relate from one to a few sources of radiation in very controlled environments. Currently, there are 111 research reactors where neutron activation analysis (NAA) is a major research and teaching component. In particular, NAA can yield a wide variety of exposures due to different types of samples and neutron fluxes. Unlike any other type of radiation laboratories, an NAA facility can contain a large variety of radioactive isotopes as a result of activation products with varying degrees of half-lives and with different intensities of gamma-rays and beta particles. Using MCNP 6.2, a Monte Carlo code developed by Los Alamos National Laboratory (LANL) for radiation transport, dose rates were computed. The computational results were validated by irradiating several National Institute of Standards and Technology (NIST) standard reference materials. The samples were allowed to decay during their transfer from the reactor to the NAA laboratory. These computational doses were validated to the experimental doses. Using this information, a database will be developed for accurately predicting the expected doses to researchers working at research reactors and develop better radiation protection standards at NAA facilities.*

Keywords: *Radiation Protection, Neutron Activation Analysis, Dose Rate, TRIGA Reactor, NIST reference materials*

1. BACKGROUND

The usage of neutron activation analysis (NAA) has been widely adopted as a non-destructive technique for characterizing elemental composition for different applications for geological, biological, environmental, archaeological and materials samples. According to the International Atomic Energy Agency (IAEA) Research Reactor Database, there are currently 224 operational research reactors in the world of which 111 are used for NAA applications [1]. The Nuclear Engineering Teaching Laboratory (NETL) at The University of Texas at Austin currently operates the newest TRIGA Mark II university reactor in the USA. The reactor has in-core irradiation facilities and five neutron beam ports with steady state operation at power levels up to 1.1 MW or pulsing mode operation up to 1.5 MW for 10 microseconds. At the center of the reactor, a maximum neutron flux of 2 x 10^{13} n cm^2 s^{-1} can be achieved. The flexibility allows the reactor to be used for numerous NAA experiments at varying reactor power, neutron flux, and irradiation times.

In a typical NAA facility, irradiated samples will yield a wide range of radioactive isotopes due to activation and nuclear decay, which have varying half-lives and different strengths of gamma rays and beta particles. This specific type of facility differs from commercial power reactors or government research laboratories in which usually workers deal with one or two types of well-characterized radiation sources. Furthermore, there is little to no guidance on radiation protection in NAA laboratories, which can lead to poor practices in handling irradiated samples. This work focuses on characterizing typical dose rates from the irradiation of NIST standard reference materials and comparing computational and experimental dose rates for a short-lived NAA facility using a typical pneumatic system. This work will be beneficial in characterizing radiation hazards when working in NAA facilities to develop standardized radiation protection guidelines.

1.1. NAA Theory

NAA is a method of determining the composition of a given sample from the major components to trace elements by exposing the sample to neutrons, usually in a reactor, but accelerators (such as DT and DD) and neutron sources (such as Pu(Be) and ^{252}CF) can also be used. In a reactor the sample will mainly undergo reactions in which a stable isotope will capture a neutron and become radioactive. The sample then undergoes nuclear β^+ or β^- decay in which particles and gamma rays are released until the radionuclides return to a stable state. The gamma rays released are unique signatures for each of the isotopes present in the sample. Using a gamma detector, the different gamma rays can be quantified to determine what is present in the sample. A typical activation process is shown in Figure 1, in which ^{59}Co is activated through neutron capture into ^{60m}Co and ^{60}Co. The figure shows a characteristic decay scheme for returning to a stable configuration.

* jparga@lanl.gov

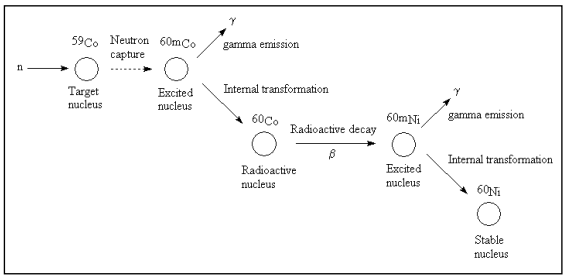

Figure 1. Neutron Activation of ^{59}Co

The activation of any given isotope is governed by the reaction rate (R) as illustrated in Equation 1.

$$R = n\sigma\Phi \quad (1)$$

The reaction rate is illustrative of how many target atoms (n) are present in the NAA sample the cross section (σ) and flux (φ) are dependent on the neutron energy. However, this does not take into account the decay that occurs during activation. Equation 2 more properly shows the number of radioactive atoms present at any time by including the decay constant (λ) and the number of radioactive atoms (N) to account for decay [2].

$$\frac{dN}{dt} = \Phi\sigma n - \lambda N \quad (2)$$

The corresponding activity for each different isotope is seen in Equation 3.

$$A(t_d) = \Sigma\Phi[1 - \exp(-\lambda t_{irr})]\exp(-\lambda t_d) \quad (3)$$

where the activity after decay is a function of the macroscopic cross section (Σ), neutron flux (Φ), decay constant (λ), irradiation time (t_{irr}), and decay time (t_d).

1.2. Important Isotopes in NAA

Table 1. Properties of Reactions Producing Short-Lived Isotopes Through (n,γ) Reactions

Element	Isotope	Half-life	γ -rays (keV)
Ag	^{110}Ag	24.6 sec	657.8
Al	^{28}Al	2.24 min	1778.9
Ba	^{139}Ba	83.2 min	165.9
Br	^{80}Br	17.7 min	616.2
Br	^{80m}Br	4.42 hr	37.1
Ca	^{49}Ca	8.7 min	3084.4
Cl	^{38}Cl	37.3 min	1642.4, 2167.5
Co	^{60m}Co	10.48 min	58.6
Cu	^{66}Cu	5.1 min	1039.4
Dy	^{165}Dy	2.33 hr	94.7
F	^{20}F	11.0 sec	1633.8
I	^{128}I	25.0 min	442.3
In	^{116m}In	54.2 min	416.9, 1097.3
K	^{42}K	12.36 hr	1524.7
Mg	^{27}Mg	9.45 min	843.8, 1014.4
Mn	^{56}Mn	2.58 hr	846.7, 1810.7
Na	^{24}Na	15.0 hr	1368.6, 2754.1
Se	^{77m}Se	17.4 sec	161.7
Sb	^{122m}Sb	4.15 min	61.5
Si(n,p)	^{29}Al	6.6 min	1273.0
Sr	^{87m}Sr	2.81 hr	388.4
Ti	^{51}Ti	5.8 min	320.1
U	^{239}U	23.5 min	74.6
V	^{52}V	3.76 min	1434.1

Typically, two different irradiations can be performed: one to determine short-lived isotopes and the other to determine medium to long lived isotopes. In this work, we focused on short-lived isotopes, as these will deliver most of the radiation when handling the samples between irradiation and counting. Previous work by the IAEA [3] focused on the short-lived isotopes shown in Table 1. These were chosen as common isotopes arising from NAA in common National Institute of Standards and Technology (NIST) Standard Reference Materials (SRM). SRMs are used for having well-established composition characterization, which is needed for accurate material modeling in MCNP 6.2.

1.3. Radiation Protection in NAA Facilities

Radiation protection standards across the world are usually derived from IAEA or country safety documents. In particular IAEA GSG-7: Occupational Radiation Protection [4] and SSR-3: Safety of Research Reactors [5] are often used. GSG-7 dictates the various occupational exposures yearly dose limits. The whole-body effective dose is set at 20 mSv per year averaged over five consecutive years and at 50 mSv in any single year. Both GSG-7 and SSR-3 documents put the responsibility for protection against occupational exposure on the employers, registrants, and licensees. The documents provide a methodology for a graded approach on optimizing radiation protection. However, no standard methodology is proposed on how to handle NAA samples.

2. METHODOLOGY

GSG-7 proposes different approaches on exposure assessment methods. This paper focuses on the use of simulations, which the IAEA states "can be powerful and can provide information instantly on the parameters that influence doses that would be received in given exposure situations. The results of simulations should be verified by measurement." Therefore, this work focuses on two different aspects: 1) developing a robust computational simulation for NAA and 2) verifying computational results with experimental results by irradiating samples.

2.1. NAA Simulation

Utilizing MCNP 6.2, a radiation transport software developed by Los Alamos National Laboratory [6], dose rates in the NETL short-lived NAA facility were calculated. The simulation was divided into two parts, one accounted for the sample irradiation inside the TRIGA reactor, and the other for the dose rates the radiation worker can expect after irradiation.

The TRIGA reactor had been previously modeled by the NETL [7]. The reactor is composed of 19.8% enriched uranium-zirconium hydride fuel, stainless steel cladding, graphite reflectors, and boron carbide control rods. In this specific model, the fuel is modeled per the last fuel shuffle on January 15, 2016. The model also includes all the experimental facilities available at NETL such as the neutron beam ports. The reactor core is shown in Figure 2.

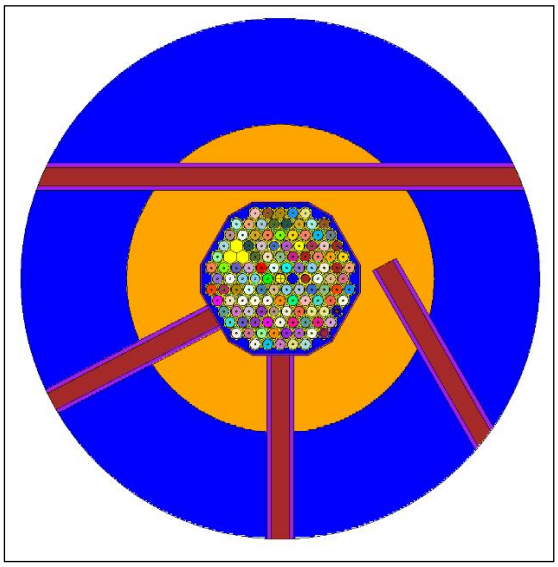

Figure 2. NETL TRIGA MCNP 6.2 Model

It was of importance to model the reactor irradiation facilities, as neutron energies will affect the activation of the sample due to neutron capture cross sections. The model needed to be modified to track material activation and decay during irradiation.

There are two main avenues for modeling the sample material activation. The first is by using the Cinder90 [8]. Cinder90 solves the Bateman equations to find the activity of isotopes by accounting for production and decay during the irradiation and decay of a sample material. The second option is to model the neutron current into the sample geometry cell in the TRIGA MCNP model. Using the surface write (SSW) card the current is written as a data file that can be used by the surface read (SSR) card. Using this information, a neutron source directed toward the material sample is modeled and the ACT card can be used to determine the dose rate from activation. The ACT card models delayed particles such as delayed neutrons and gammas.

The materials modeled are four NIST SRMs: Peach Leaves (1547), Trace Elements in Coal (1632d), Trace Elements in Coal Fly Ash (1633c), and Montana I Soil (2710a). The materials represent typical soils, vegetation and contaminated geological samples that are analyzed at NETL [9-12]. The materials are described using elemental mass fractions, but in order to run in MCNP 6.2 the materials need to be specified as isotopic mass fractions. This was done by multiplying the isotopic abundance by the elemental mass given in the SRM certificates for each element. The next step was to verify that each isotope was included in the neutron continuous-energy cross sections library from the List of Available ACE Data Tables [13].

The ACT card is used to obtain a dose rate from the sample after the irradiation. This information was used as the source information for the dose rate model. In previous work by [14-15], a mathematical phantom developed by Oak Ridge National Laboratory (ORNL) was used for organ dose modeling. For this work, we utilized PIMAL, a mathematical phantom software [16] developed by the Nuclear Regulatory Commission (NRC), based on the ORNL phantom with the added ability to manipulate the extremities as seen in Figure 3. It was of importance to model the position of the extremities, as this is the usual position radiation workers will use when handling NAA samples.

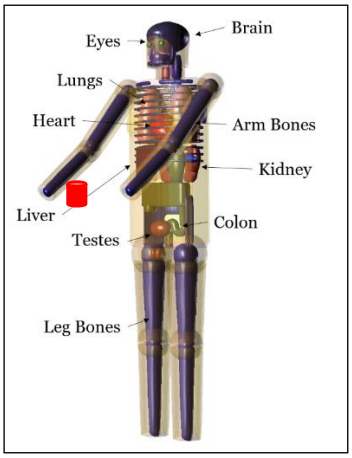

Figure 3. NRC PIMAL Phantom

The PIMAL phantom allows for dose calculations by utilizing an MCNP F6 energy deposition tally. The phantom tallies information on 23 different organs ranging from the brain, to the lungs to the testes. This tally gives information in [MeV/gram] which was converted to units of [Gray] to determine the absorbed dose in each individual organ.

2.2. Experimental Work

It is of importance to validate computational results by leveraging experimental results. To accurately compare these two methods, NIST SRM samples were prepared by weighing approximately 0.50 grams and encapsulating the sample inside the standard plastic sample holder. The samples were irradiated in the TRIGA Reactor at two different power levels for 10 seconds as shown in Table 2.

Table 2. NIST SRM Samples Irradiation Data

NIST SRM	Weight (g)	Power (kW)	β and γ Dose Rate on Contact	γ Dose Rate on Contact
1633c	0.52869	950	0.21 Gy/hr	19 mGy/hr
1632d	0.54485	950	9.6 mGy/hr	1.2 mGy/hr
2710a	0.52474	100	8.6 mGy/hr	1.2 mGy/hr
1547	0.38093	950	3.6 mGy/hr	0.56 mGy/hr

The exposure rates were captured using a Victoreen 450B survey meter pressed against the sample immediately after irradiation and converted to dose rates. To measure only the gamma dose, the beta slide shield was used. After surveying the samples, they were allowed to decay for a short period, on the order of minutes, before conducting gamma spectroscopy.

To conduct gamma spectroscopy, the system was calibrated to a D (10 cm) and DD (20 cm) sample holder. These distances minimize any summing effects. This

was done by placing an ^{152}Eu standard source and counting it for a determined period. The source was certified at an activity of 3700 Bq on July 27, 2006. Using EG&G Maestro, a multi-channel analysis (MCA) software, the net counts under each peak were obtained and compared to the number of expected gammas. The number of expected gammas is calculated by accounting for decay of the standard source and for the yield of each specific gamma-ray. The ratio of actual gammas to expected gammas yields the absolute detector efficiency [17].

The efficiency curves, Figure 4 and Figure 5, were used to characterize the detector efficiency response at different energies. In both configurations, the efficiency calibration yielded a good correlation between absolute detector efficiency and energy with an R^2 above 0.99 for both cases. It should be noted that interpolation can be safely done but caution should be used when extrapolating. It can be seen that the absolute efficiency for the DD sample holder calibration is about an order of magnitude smaller than the D sample holder. This is due to the doubling in distance from the HPGe detector.

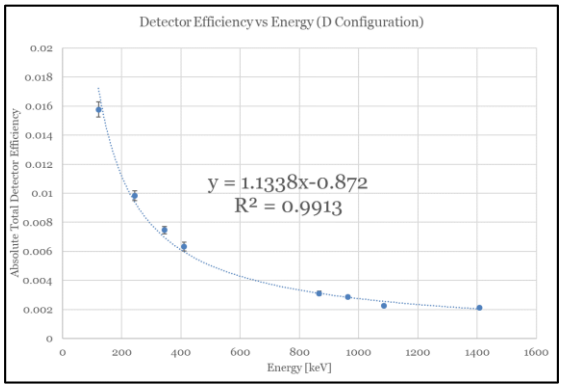

Figure 4. Detector Efficiency Calibration D (10 cm) Configuration

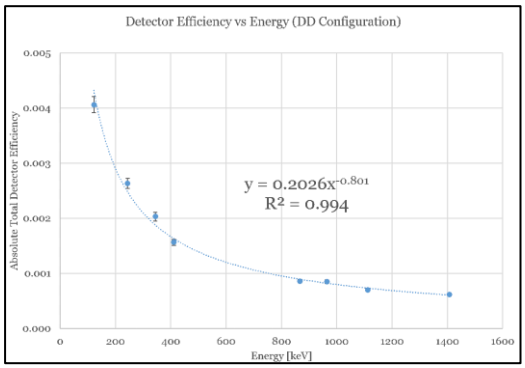

Figure 5. Detector Efficiency Calibration DD (20 cm) Configuration

The activity for each peak can be calculated as a function of net counts, absolute efficiency, and yield. The net counts were obtained from Maestro MCA software by marking regions of interest (ROI).

3. Results

3.1. Experimental Results

Table 3 shows the peak activities in Becquerel for the different isotopes discussed in Table 1. It should be noted that some of the isotopes could not be discerned from the background continuum, therefore information is not reported.

Table 3. Experimental Isotopic Activities for Short-Lived Isotopes[1] in NIST SRMs Immediately After Irradiation

Isotope	Energy (keV)	NIST SRM Sample Activity (Bq)			
		1547	1633c	1632d	2710a
^{110}Ag	657.8	0.00E+00	0.00E+00	0.00E+00	0.00E+00
^{28}Al	1778.9	0.00E+00	4.72E+10	9.04E+09	2.10E+09
^{139}Ba	165.9	3.31E+03	1.02E+04	1.52E+02	0.00E+00
^{80}Br	616.2	1.45E+05	1.29E+04	3.82E+04	0.00E+00
^{80m}Br	37.1	0.00E+00	0.00E+00	0.00E+00	0.00E+00
^{49}Ca	3084.4	2.77E+03	0.00E+00	1.10E+03	0.00E+00
^{38}Cl	1642.4	4.04E+04	0.00E+00	2.87E+04	0.00E+00
^{38}Cl	2167.5	4.04E+04	0.00E+00	2.82E+04	0.00E+00
^{60m}Co	58.6	0.00E+00	0.00E+00	4.08E+04	0.00E+00
^{66}Cu	1039.4	1.06E+06	0.00E+00	0.00E+00	1.33E+06
^{165}Dy	94.7	2.05E+04	1.21E+05	5.52E+03	1.17E+03
^{20}F	1633.8	0.00E+00	0.00E+00	0.00E+00	0.00E+00
^{128}I	442.3	0.00E+00	1.19E+03	2.84E+03	0.00E+00
^{116m}In	416.9	0.00E+00	1.46E+03	0.00E+00	9.40E+03
^{116m}In	1097.3	0.00E+00	3.46E+03	0.00E+00	9.36E+03
^{42}K	1524.7	8.21E+04	1.35E+04	0.00E+00	0.00E+00
^{27}Mg	843.8	0.00E+00	0.00E+00	0.00E+00	1.03E+06
^{27}Mg	1014.4	4.89E+05	8.20E+05	6.89E+04	1.79E+05
^{56}Mn	846.7	1.72E+05	0.00E+00	0.00E+00	7.83E+04
^{56}Mn	1810.7	1.65E+05	9.47E+04	5.28E+03	7.56E+04
^{24}Na	1368.6	1.48E+03	1.01E+04	1.98E+03	5.18E+03
^{24}Na	2754.1	1.37E+03	9.56E+03	1.87E+03	4.53E+03
^{77m}Se	161.7	0.00E+00	0.00E+00	0.00E+00	0.00E+00
^{122m}Sb	61.5	0.00E+00	0.00E+00	0.00E+00	0.00E+00
^{29}Al	1273	0.00E+00	0.00E+00	0.00E+00	7.40E+04
^{87m}Sr	388.4	5.36E+02	1.64E+03	1.09E+02	0.00E+00
^{51}Ti	320.1	0.00E+00	4.27E+05	3.42E+04	1.87E+04
^{239}U	74.6	9.47E+02	8.17E+03	4.60E+02	1.08E+03
^{52}V	1434.1	0.00E+00	4.56E+07	7.26E+06	1.17E+06

[1] values of 0.00 indicate the gamma-ray was not detected or used.

Furthermore, these results were corrected to account for the decay time and the counting time to yield the activity immediately after irradiation. It can be seen that the major contributors to activity across the different SRM samples were ^{28}Al, ^{52}V, ^{165}Dy, ^{27}Mg, ^{139}Ba, ^{80}Br, ^{128}I, ^{116m}In, ^{42}K, ^{87m}Sr, ^{51}Ti, and ^{239}U. There are some variations between the activity levels in SRM 2710a to the other samples as this sample was irradiated at a significantly lower power level due to the known activity levels with activation products in this sample.

3.2. Computational Results

It was of importance to understand the neutron spectrum experienced in the pneumatic irradiation facility. Utilizing an MCNP F4 tally the neutron flux in [#/cm^2] was obtained which was then converted to [n/cm^{2}s] by normalizing by the source [n/s].

The dose rates for the PIMAL phantom are shown in Table 4 for SRM 1633c. It can be seen that the relative error for five of the tallies was above 10%. This is likely due to not enough particles scoring in these tallies due to attenuation in other organs. Specifically, the tallies with the higher relative errors tend to be further away and deeper within the phantom. The organs with the higher absorbed dose rate were those closest to the irradiated sample such as the testes, urinary bladder,

prostate, colon, small intestine, and stomach. It should be noted that the absorbed dose rate for the skin and muscle accounts for the entire phantom.

Table 4. SRM 1633c Absorbed Dose Rates

Organ	Absorbed Dose Rate (Gy/hr)	Relative Error (%)
Testes	0.0156	4.29
Urinary Bladder	0.0146	2.74
Prostate	0.0140	6.35
Colon	0.0137	1.63
Small Intestine	0.0109	1.9
Stomach	0.0097	3.14
Muscle	0.0070	0.99
Skin	0.0050	1.05
Pancreas	0.0046	4.87
Spleen	0.0046	5.04
Bone Surface	0.0038	1.44
Bone Marrow	0.0036	1.45
Kidneys	0.0031	4.21
Liver	0.0022	3.04
Adrenals	0.0021	15.46
Breast	0.0014	7.59
Lungs	0.0013	3.36
Esophagus	0.0011	10.18
Thymus	0.0010	23.72
Thyroid	0.0003	34.13
Extra Thoracic Airways	0.0003	23.99
Eyes	0.0002	40.46
Brain	0.0001	11.96
Total	**0.1203**	**-**

4. Discussion

The computational total absorbed dose rate of 0.12 Gy/hr is within 40% of the observed experimental value of 0.21 Gy/hr (see Table 2). However, this discrepancy can be explained by the experimental value being obtained on direct contact with the sample while the computational dose rate accounted for the distance between the phantom and the irradiated sample. Furthermore, to have higher confidence in tallies with large relative errors, more time should be invested in variance reduction methods to bias the particles to these further away regions. These could be done with the use of weight windows and source biasing. In future development it would also be of interest to computationally model the isotopic concentration and activities to compare the results to the gamma spectroscopy results. This was attempted using Cinder90, however the package released by the Radiation Safety Information Computational Center (RSICC) only works with MCNPX. Through further research this task can likely be achieved with Cinder2008 which is the successor of Cinder90 and has compatibility with MCNP6.

5. Conclusion

Through this paper we established a methodology on modeling NAA irradiation runs to determine the expected dose rates when handling the samples. Experimental work was also conducted to verify the computational results, which are within 40% agreement. Clearly, the absorbed beta dose rate is of major significance and should never be underestimated. Furthermore, absorbed dose rates for only a hand should be developed.

This approach will be useful in developing a database of standard environmental, geological, biological and engineering materials which are commonly irradiated at NETL to develop radiation protection guidelines. These guidelines can then be used to create standard operating procedures to minimize the dose incurred by the NAA laboratory staff.

Acknowledgements: *The authors would like to thank the Nuclear Engineering Teaching Laboratory at The University of Texas at Austin for allowing us to utilize their NAA facilities for this research. Furthermore, we would like to acknowledge Radiation Safety Information Computational Center (RSICC) at Oak Ridge National Laboratory for their support in providing the different codes utilized in this paper.*

References

1. *Research Reactor Database*, IAEA, Vienna, Austria, 2019.
   Retrieved from: https://nucleus.iaea.org/RRDB/Content/Util/NAA.aspx
   Retrieved on: Jun. 17, 2019
2. H. Cember, T. E. Johnson, "Interaction of Radiation with Matter," in *Introduction to Health Physics*, 4th ed., New York (NY), USA: McGraw-Hill, 2009, ch. 5, pp. 192 – 193.
   Retrieved from: http://93.174.95.29/_ads/0EF2AF24D5751F8535C0FDEE9BE39D48
   Retrieved on: Aug. 12, 2019
3. *Sampling and Analytical Methodologies for Instrumental Neutron Activation Analysis of Airborne Particulate Matter*, Training Course Series No. 4, IAEA, Vienna, Austria, 1992.
   Retrieved from: https://www.iaea.org/publications/346/sampling-and-analytical-methodologies-for-instrumental-neutron-activation-analysis-of-airborne-particulate-matter
   Retrieved on: Aug. 12, 2019
4. *Occupational Radiation Protection*, Safety Standards Series No. GSG-7, IAEA, Vienna, Austria, 2018.
   Retrieved from: https://www.iaea.org/publications/11113/occupational-radiation-protection
   Retrieved on: Aug. 12, 2019
5. *Safety of Research Reactors*, Safety Standards Series No. SSR-3, IAEA, Vienna, Austria, 2016.
   Retrieved from: https://www.iaea.org/publications/11031/safety-of-research-reactors
   Retrieved on: Aug. 12, 2019
6. C. J. Werner et al., *MCNP6.2 Release Notes*, Los Alamos National Laboratory, Los Alamos (NM), USA, 2018.
   Retrieved from: https://laws.lanl.gov/vhosts/mcnp.lanl.gov/pdf_files/la-ur-18-20808.pdf
   Retrieved on: Jul. 15, 2019
7. W. Charlton, "NETL TRIGA Input Deck," Unpublished.

8. M. L. Fensin, J. S. Hendricks, G. W. McKinney, "Monte Carlo Burnup Interactive Tutorial," presented at the *ANS 2009 Student Meeting*, Gainesville (FL), USA, Apr. 2009.
Retrieved from:
https://mcnp.lanl.gov/pdf_files/la-ur-09-2051.pdf
Retrieved on: Apr. 12, 2019
9. *Peach Leaves*, SRM 1547, Apr. 2, 2019.
Retrieved from:
https://www-s.nist.gov/srmors/certificates/1547.pdf
Retrieved on: Apr. 12, 2019
10. *Trace Elements in Coal*, SRM 1632D, Oct. 14, 2014.
Retrieved from:
https://www-s.nist.gov/srmors/certificates/1632d.pdf
Retrieved on: Apr. 12, 2019
11. *Trace Elements in Coal Fly Ash*, SRM 1633C, Jun. 23, 2011.
Retrieved from:
https://www-s.nist.gov/srmors/certificates/1633C.pdf
Retrieved on: Apr. 12, 2019
12. *Montana I Soil*, SRM 2710A, Nov. 2, 2018.
Retrieved from:
https://www-s.nist.gov/srmors/certificates/2710a.pdf
Retrieved on: Apr. 12, 2019
13. J. L. Conlin, *Listing of Available ACE Data Tables: Formerly Appendix G of the MCNP Manual*, Los Alamos National Laboratory, Los Alamos (NM), USA, 2017.
Retrieved from:
https://laws.lanl.gov/vhosts/mcnp.lanl.gov/pdf_files/la-ur-17-20709.pdf
Retrieved on: Jul. 15, 2019
14. S. Landsberger, A. Sharp, S. Wang, Y. Pontikes, A. H. Tkaczyk, "Characterization of bauxite residue (red mud) for 235U, 238U, 232Th and 40K using neutron activation analysis and the radiation dose levels as modeled by MCNP," *J. Environ. Radioact.*, vol. 173, pp. 97 – 101, Jul. 2017.
DOI: 10.1016/j.jenvrad.2016.12.008
PMid: 28049554
15. S. Wang, S. Landsberger, "MCNP modeling of NORM dosimetry in the oil and gas Industry," *J. Radioanal. Nucl. Chem.*, vol. 309, no. 1, pp. 367 – 371, Jul. 2016.
DOI: 10.1007/s10967-016-4781-x
16. *PIMAL: Phantom with Moving Arms and Legs*, Nuclear Regulatory Commission, Oak Ridge (TN), USA, 2017.
Retrieved from:
https://ramp.nrc-gateway.gov/PIMAL
Retrieved on: Apr. 12, 2019
17. G. F. Knoll, *Radiation Detection and Measurement*, 3rd ed., Hoboken (NJ), USA: John Wiley & Sons, Inc., 2000.
Retrieved from:
https://libgen.is/book/index.php?md5=51A49204DB42FB158A457EADB9FB7239
Retrieved on: Jun. 19, 2019